Size and Alloying Extent Dependent Physiochemical Properties of Pt−Ag/C Nanoparticles Synthesized by the Ethylene Glycol Method

ARTICLE *in* THE JOURNAL OF PHYSICAL CHEMISTRY C · FEBRUARY 2008

Impact Factor: 4.77 · DOI: 10.1021/jp077138p

Size and Alloying Extent Dependent Physiochemical Properties of Pt−Ag/C Nanoparticles Synthesized by the Ethylene Glycol Method

Bing Joe Hwang,*,†,‡ Sakkarapalayam Murugesan Senthil Kumar,† Ching-Hsiang Chen,†,§ Ren-Wen Chang,† Din-Goa Liu,‡ and Jyh-Fu Lee‡

Nanoelectrochemistry Laboratory, Department of Chemical Engineering, National Taiwan University of Science and Technology, Taipei 106, Taiwan

Received: September 5, 2007

Bimetallic alloy nanoparticles consisting of two noble metals Pt−Ag supported on carbon with a variable dimension were successfully prepared by ethylene glycol (EG) synthesis method. This work highlights the viability of EG synthesis methodology yielding a range of particle size from 1.2 to 3.1 nm with 1:1 atomic composition but with different alloying extents by a simple control over the solution pH of the preparation medium. The physical properties of resultant Pt−Ag/C nanoparticles such as size, structure, composition, coordination, and alloying extent parameters as well as d-band unfilled states of Pt atom were systematically studied by X-ray diffraction (XRD), energy dispersive X-ray analysis (EDX), transmission emission microscopy (TEM), and X-ray absorption spectroscopy (XAS) techniques. Both EDX and XAS analysis confirmed that the catalyst composition was nearly the same as that of the nominal value. It was realized that the lower preparation pH produces the Pt−Ag/C with larger dimension, wider particle size distribution (PSD), and worse alloying extent associated with lower d-band unfilled states. At higher preparation pH yields Pt−Ag/C particles of smaller size, narrower PSD, and better alloying extent along with higher d-band unfilled states. Increasing the d-band unfilled states of the bimetallic Pt−Ag/C nanoparticles leads to a negative shift in CO oxidation peak potential at identical experimental conditions. The observed d-band unfilled state of the Pt atom in the Pt−Ag/C nanoparticles may be due to the resultant of the two opposite effects, namely, the electron donation by Ag and the size effect of the Pt−Ag nanoparticles. The electron donation ability of Ag is believed to associate with the alloying extent of Ag and/or Pt atoms in the Pt−Ag nanoparticles, and a possible explanation was drawn on the basis of their charge transfer index scale values.

Introduction

Noble metal nanoparticles are considered as the most attractive materials in "nanotechnology" or "nanobiotechnology" because of their promising as well as wide ranging applications. Such a privilege for these materials is due to their interesting optical, electrical, magnetic, physicochemical, and chemical properties.[1−7] More recently, particular interests are focused in bimetallic nanoparticles, which exhibit unique characteristics that are not just the addition of the two properties of the constituent metals.[6] Bimetallic nanoparticles can be obtained as alloy or core shell particles to provide the latitude required for property tuning according to the needs of the intended application.[8−12] In general, bimetallic nanoparticles can be prepared by the simultaneous or successive reduction of the two metal precursor ions in the presence of a suitable stabilizer. The simultaneous reduction method may produce a particle structure between core−shell and homogeneous alloy depending on the reduction conditions.[13−15] The growth of the core−shell structure can be accomplished by the successive reduction of one metal ion over the core of the other metal.[10,16]

Torigoe et al.[17] reported that the chemical reduction of silver-(I) bis(oxalato)palatinate(II) successfully provides Pt−Ag alloy colloids. They proved that the reduction of $[Pt(C_2O_4)_2]^{2-}$ takes place by the catalytic action of the preformed Ag particles to form the Pt−Ag alloy. In another report, Liz-Marzan and Philipse[18] demonstrated the ability to form Pt−Ag bimetallic nanoparticles inside the imogolite fibers without any other stabilizers. Their optical property study proves that the Pt−Ag particles consist of layers of the metals rather than a mixture at the atomic level. Apart from this, an approach based on radiolysis synthesis by using γ-ray irradiation was also used for the preparation of Pt−Ag bimetallic nanoparticles.[19,20] But the authors' transmission emission microscopy (TEM) and X-ray absorption spectroscopy (XAS) studies proves that their method is only able to produce a Pt−Ag nanowire of Ag core and Pt shell structure. They concluded that due to a higher positive reduction potential of Ag^+/Ag^0 compared to Pt^{4+}/Pt^0 the formation of a Ag cluster is always preferred over Pt. Eventually the process ends up with Ag core Pt shell structure formation. In this context it should be noted that it is almost an unlikely process to produce a well-mixed Pt−Ag alloy via the usual simultaneous reduction process of Pt and Ag precursors.

Recently, Bock et al.[21] have demonstrated that Pt−Ru/C bimetallic nanoparticles can be prepared by employing ethylene glycol as a reducing agent. Particle sizes can be found in a wide range from 0.7 to 4 nm by fine control over the pH of the reaction medium. The main advantages of this EG method are (i) ease of performance, (ii) no requirement for the addition of protective polymers to stabilize the particles, (iii) performance

* Corresponding author. E-mail: bjh@mail.ntust.edu.tw.
† National Taiwan University of Science and Technology.
‡ National Synchrotron Radiation Research Centre, Hsinchu 300, Taiwan.
§ Institute of Atomic and Molecular Sciences, Academia Sinica, Taipei 115, Taiwan.

10.1021/jp077138p CCC: $40.75
Published on Web 01/31/2008

at room temperature, and (iv) particle depososition on Vulcan XC-72 carbon in a convenient process. Following this study, we have probed the formation mechanism of Pt−Ru/C nanoparticles by employing in-situ X-ray absorption spectroscopy for the above system to control the distribution and stability of the resultant nanoparticles.[22] We realized from the above study that the solution pH will have a fine control over the reduction rate of the noble metals of Pt and Ru, which in turn enhances the atomic distribution in the Pt−Ru/C nanoparticles. It has been realized that the unequal reduction rates of two noble metals are encountered in the formation of well-mixed Pt−Ag nanoparticles. This has necessitated studying the effect of pH on the particle size as well as alloying extent values of the resultant Pt−Ag/C nanoparticles. In this paper we intended to establish the EG-based polyol process for Pt−Ag/C nanoparticle preparation. Further we extended our examination to CO stripping experiments on resultant Pt−Ag/C nanoparticles to probe the real impact of their size and alloy extent values.

To study the alloying extent of the bimetallic Pt−Ru/C nanoparticles, we have successfully utilized the X-ray absorption fine structure (XAFS) technique.[23] The wide ranges of applications of the XAS technique for bimetallic nanoparticles are evidenced from numerous literature reports,[24−31] and our group is actively involved in demonstrating XAS to probe the formation mechanism as well as structural changes in nanoparticles.[32−36] The analysis is based on a fitting of the complex Fourier transform of the XAFS oscillations, revealing quantitative information about coordination numbers (N), bond lengths (r), and bond-length distribution (Debye−Waller factor) (σ^2) of the neighboring atoms. Unlike diffraction, XAFS does not require a high degree of crystallinity or long-range ordering in a sample. Hence, the technique is particularly useful to extract structural information from disordered systems, such as amorphous powders or nanoparticles. The part of the XAFS spectrum around the edge energy, called X-ray absorption near-edge structure (XANES), can be used to determine the oxidation state of the absorbing atom. A change in the oxidation state is reflected in a shift in the edge energy (from the pure metallic value) and whiteline features. Moreover, this region provides information about the fractional d-electron density and electronic environment of the absorbing atom.[23]

In the light of these earlier reports, this paper aims to investigate the influence of solution pH on the alloying extent and d-band unfilled state of the resultant Pt−Ag/C nanoparticles prepared by an EG method. The XAS technique has been employed to determine the above-mentioned properties of nanoparticles. Apart from this, we have attempted to correlate the relation between the d-band unfilled states and the CO oxidation activity for the Pt−Ag/C nanoparticles by implementing electrochemical CO stripping experiments.

Experimental Section

Preparation of Carbon-Supported Pt−Ag Nanoparticles by the Ethylene Glycol (EG) Method. A solution of 3×10^{-4} M $H_2Pt(OH)_6$ in 30 mL of EG solution was mixed with 3×10^{-4} M $AgNO_3$ dissolved in 30 mL of EG, and the solution was allowed for 10 min to stand at constant pH value ≈ 2. In the next step the required pH of the mixture was adjusted to 4, 6, 8, and 10 by adding 0.1 M NaOH solution. The resultant mixtures were placed in a microwave reactor at 160 W power and 160 °C for about 20 min. After this the obtained mixtures were added with 0.212 g of Vulcan XC-72 and placed in an ultrasonic bath for about 30 min. Finally the reaction mixture was washed by employing a high power centrifugal pump at 18 000 rpm for 30 min. This process was repeated for five times for a complete removal of all the organic residue materials in the mixture. After washing, all the samples obtained were dried at 70 °C in an air oven for about 16 h.

XRD, EDX, and TEM Measurements. Powder X-ray diffraction (XRD) patterns for the E-tek Pt/C and Pt−Ag/C samples were obtained on a diffractometer (Rigaku Dmax-B, Japan) using a Cu Kα source that was operated at 40 kV and 100 mA. The X-ray diffractogram was obtained at a scan rate of 0.05 deg s^{-1} for 2θ values between 20 and 90°. The EDX measurements were performed with a JSM 6500 EDX analyzer. Transmission electron microscopy (TEM) examination was performed on a JEOL JEM-1010 microscope that was operated at an accelerating voltage of 200 kV. Specimens were prepared by ultrasonically suspending the nanoparticles in ethanol, which were then applied to a copper grid and dried in air.

XAS Measurements. The X-ray absorption spectra were recorded at the National Synchrotron Radiation Research Centre (NSRRC) of Taiwan, Beam Line 01 C. The electron storage ring was operated at 1.5 GeV with 300 mA. A double Si(111) crystal monochromator was employed for energy selection with a resolution $\Delta E/E$ better than 1×10^{-4} at both the Pt L_{III}-edge (11 564 eV) and the Ag K-edge (25 514 eV). All the experiments for bimetallic nanoparticles were conducted in a homemade cell made of stainless steel for the XAS study. Two holes were made in the cell. After placement of the solid samples, the holes were closed with a Kapton film cap to avoid the exposure of the sample to the outer atmosphere. Before measurement of the XAS, the sample was reduced with 10% H_2 for 30 min to remove the surface oxygen. The total amount of the sample was adjusted to reach the optimum absorption thickness ($\Delta\mu x = 1.0$; $\Delta\mu$ is the absorption edge and x is the thickness of the sample) so that the proper edge jump step could be achieved during the measurements. All of the spectra were recorded at room temperature in a transmission mode. Higher harmonics were eliminated by detuning the double-crystal Si(111) monochromator. Three gas-filled ionization chambers were used in series to measure the intensities of the incident beam (I_0), the beam transmitted by the sample (I_t), and the beam subsequently transmitted by the reference foil (I_r). The third ion chamber was used in conjunction with the reference sample, which was a Pt foil for Pt L_{III}-edge measurements and Ag foil for Ag K-edge measurements. The control of parameters for EXAFS measurements, data collection modes, and calculation of errors were all done as per the guidelines set by the International XAFS Society Standards and Criteria Committee.[37]

EXAFS Data Analysis. The XAS experimental data were treated by utilizing the standard procedures. The EXAFS function, ø, was obtained by subtracting the postedge background from the overall absorption and then normalized with respect to the edge jump step. The normalized $\chi(E)$ was transformed from energy space to k-space, where "k" is the photoelectron wave vector. The $\chi(k)$ data were multiplied by k^2 to compensate for the damping of EXAFS oscillations in the high-k region. Subsequently, k^2-weighted $\chi(k)$ data in k-space ranging from 3.61 to 12.74 $Å^{-1}$ for the Pt L_{III}-edge and from 3.6 to 12.17 $Å^{-1}$ for the Ag K-edge were Fourier transformed (FT) to r-space to separate the EXAFS contributions from the different coordination shells. A nonlinear least-squares algorithm was applied to the curve fitting of an EXAFS in the r-space between 1.8 and 3.5 Å for both Pt and Ag depending on the bond to be fitted. The Pt−Ag reference file was determined by a theoretical calculation. Reference phase and amplitude for the Pt−Pt absorber−scatterer pairs were obtained from a Pt foil.

TABLE 1: Composition and Grain Size of the Commercial Pt/C (E-tek) and Pt−Ag/C Nanoparticles Prepared by the EG Method

catalyst	Pt:Ag	grain size (nm) from XRD	grain size (nm) from TEM
Pt/C (E-tek)	0	2.1	2−3
Pt−Ag/C (pH = 4)	48.7:51.3	3.1	2−3
Pt−Ag/C (pH = 6)	49.0:51.0	2.7	2−3
Pt−Ag/C (pH = 8)	48.1:51.9	2.4	2−3
Pt−Ag/C (pH = 10)	50.5:49.5	1.2	1−2

For the Ag−Ag absorber−scatterer pair, the phase and amplitude were obtained from reference Ag foil. All the computer programs were implemented in the UWXAFS 3.0 package[38] with the backscattering amplitude and the phase shift for the specific atom pairs being theoretically calculated by using the FEFF7 code.[39] From these analyses, structural parameters such as coordination numbers (N), bond distance (R), and the Debye−Waller factor (σ_j^2) and inner potential shift (ΔE_0) have been calculated. The amplitude reduction factor, S_0^2, values for Pt and Ag were obtained by analyzing the Pt and Ag foil samples and by fixing the coordination number in the FEFFIT input file. The S_0^2 values were found to be 0.905 and 0.746 for Pt and Ag, respectively.

Electrode Preparation and CO Stripping Experiments. Millipore water (18 MΩ) and sulfuric acid (Acros) were used in this study. All the experiments were carried out at ambient temperature of 25 ± 1 °C, unless stated otherwise. A conventional three-electrode electrochemical cell was used for the cyclic voltammetry (CV) measurements, with a high surface area Pt counter electrode and a saturated calomel electrode (SCE) reference (all potentials in this paper are quoted with respect to the reversible hydrogen electrode (RHE)), powered by a Solartron (1480 model) potentiostat/galvanostat. The working electrode was made of the carbon-supported Pt and Pt−Ag catalyst immobilized on a glassy carbon electrode (GCE) surface (0.1964 cm^2 area). The procedure for the electrode fabrication involved, first, the preparation of a clear suspension by sonicating a known amount of Pt/C and Pt−Ag/C powder dispersed in 0.5% Nafion, second, placing an aliquot of the suspension (7 μL of 6.2 μg of Pt mL^{-1} of the catalyst) on the GCE disc, and, third, air-drying about 5 min at room temperature and then at 80 °C to yield a uniform thin film of the catalyst. After fabrication the electrodes were immersed in N_2-saturated 0.5 M sulfuric acid and the potential was scanned from 0.05 to 1 V (RHE) about 10 cycles at a scan rate of 0.05 V s^{-1}. Next to pretreatment the CO gas was adsorbed by bubbling CO gas for 30 min at a constant potential of 0.05 V and then the dissolved CO was removed by purging N_2 gas for 15 min. The CO stripping experiment was carried out in an N_2 atmosphere at a scan rate of 0.005 V s^{-1}.

Results and Discussion

Detailed characterization of the nanoparticle composition, size, and morphology is essential to understand as well as evaluate the mechanism and viability of the preparation methodology. The composition of the Pt−Ag/C nanoparticles was determined from EDX analysis, and the values are shown in Table 1. It was found that the atomic composition of Pt−Ag is very close to the nominal value (1:1) for all the nanoparticles prepared by EG method. It is worth to mention that the values are in good agreement with the values determined by the Pt L_3 and Ag K-edge jump from the XANES measurements.

Figure 1 represents the comparison of the XRD patterns of E-tek Pt/C and the Pt−Ag/C nanoparticles prepared by the EG method at various pH values. The peak featured at about 24.8° in all the XRD patterns is originated from the Vulcan XC-72 carbon support. The formation of a homogeneous Ag−Pt alloy would lead to an expansion of the lattice parameter of Pt, as expected from Vegard's law and experimentally observed by Torogoe et al.[17] for Pt−Ag colloids. When compared with the monometallic Pt and Ag, the bimetallic Pt−Ag nanoparticles show the scattering peaks at 38.6 and 45.5° for (111) and (200) planes, respectively. Although the two peaks are very broad, the peak position of the (111) plane clearly indicates that an intermediate scattering angle between those of the monometallic metal Pt (JCPDS card: 04-0802) and Ag (JCPDS card: 87-0597) particles is evidence that all the catalysts are principally single-phase solid solutions.

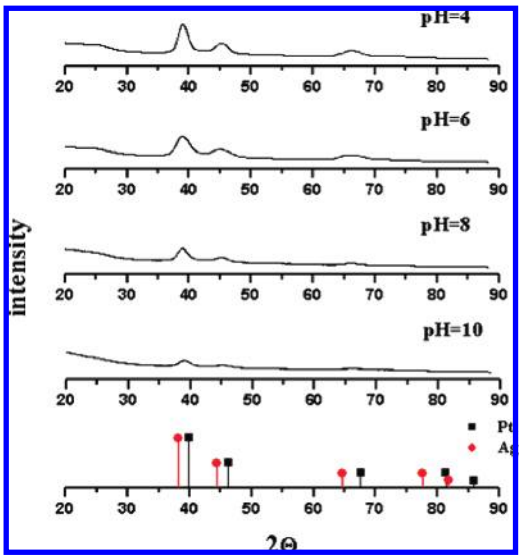

Figure 1. XRD patterns of Pt−, Ag−, and Pt−Ag alloy nanoparticles supported on carbon.

Since XRD is a grain size sensitive technique, the larger grain within the samples would produce the narrower diffraction peaks. Thus, the broad diffraction peaks observed for the Pt−Ag/C nanoparticles (pH = 10) suggest that the increase of solution pH significantly reduces their grain size. The obtained grain size values are included in Table 1. It is clear that the grain size gradually decreases with increasing pH.

The particle size and particle size distributions are clearly observed in their corresponding TEM images of the Pt−Ag/C nanoparticles as shown in Figure 2. This trend suggests that the size of the Pt−Ag catalysts can be controlled by varying the pH of the preparation medium. It is found that the catalyst size decreases with an increase in pH from 4 to 10, and the values are included in Table 1. It is well-known that the glycolate generated from the oxidation of EG associated with the reduction of metal ions will be beneficially utilized as a stabilizer to avoid particle agglomeration. Meanwhile, the ionization of glycolate increases with pH. The higher the pH is, the better the stabilizing ability of glycolate. Initial low pH value of 4 may be likely to produce Pt−Ag nanoparticles with large diameter due to their agglomeration resulting from less availability and stabilizing ability of glycolate. This situation leads to the large grain size of Pt−Ag nanoparticles with wide PSD. In contrast to this, a large amount of glycolate is produced due to the fast oxidation reactions of EG at pH = 10. This results in Pt−Ag nanoparticles with small grain size along with narrow PSD.

XANES spectra contain information on the local atom symmetry and density of states of metals and alloys. Figure 3

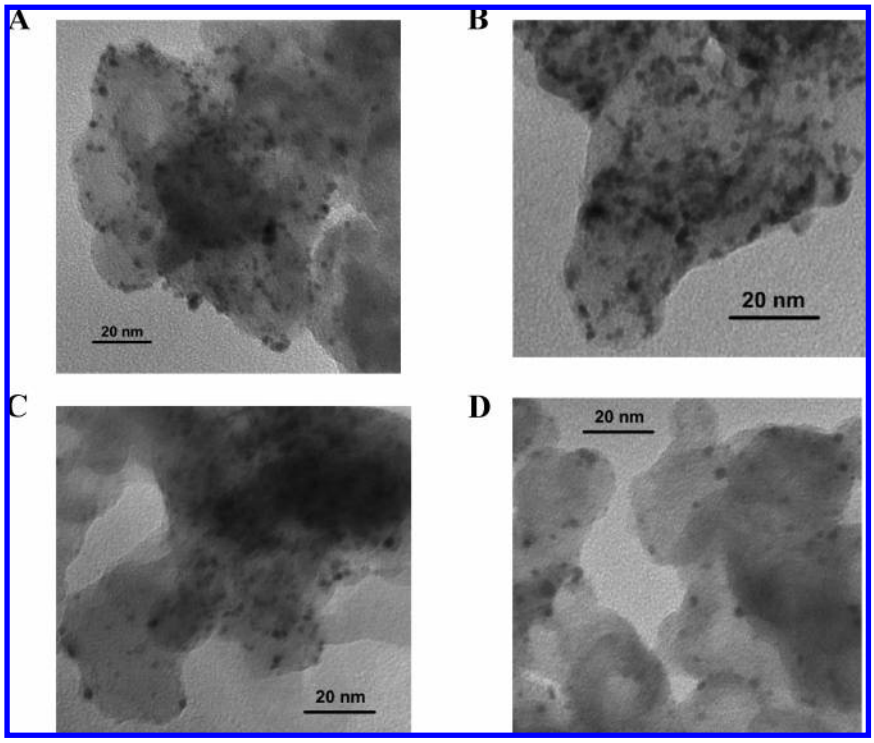

Figure 2. Typical HRTEM images of Pt−Ag/C nanoparticles prepared at (A) pH = 4, (B) pH = 6, (C) pH = 8, and (D) pH = 10 by the EG method.

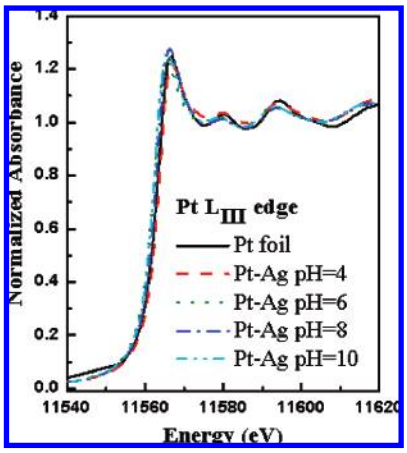

Figure 3. XANES spectra at the Pt L_{III}-edge for Pt foil and Pt−Ag/C nanoparticles prepared by the EG method.

shows these spectra at the Pt L_{III}-edge, for a Pt foil reference and the Pt−Ag/C nanoparticles prepared by the EG method. The peak centered at ca. 11 564 eV is due to the excitations of $2p_{3/2}$ electrons to empty 5d orbitals (white line), which are superimposed to $2p_{3/2}$-to-continuum transitions. Thus, the intensity of white line transitions should increase with the increase of d-band vacancy.[40] It is seen that the XANES spectra for the Pt−Ag/C nanoparticles present higher intensity than that of Pt foil. This in principle can be caused by the size effect and/or the electronic effect induced by Ag atoms. It is worthwhile to mention that the white line intensities for all the Pt−Ag/C samples are significantly lower than that of E-tek Pt/C although their particle sizes are comparable (data not shown). It could be caused by the alloying of Ag with Pt leading to a high electron density around Pt atoms. This phenomenon causes a decrease in the Pt d-band vacancy, and in turn a decrease in white line was observed for the Pt−Ag/C nanoparticles.

To quantify the above said differences in the white line intensity between the catalysts and platinum foil, a method modified by Reifsnyder et al.,[41] which was originally developed by Mansour et al.,[42] was adopted in this work. After subtraction of the platinum foil data from the catalyst data, the resulting curves were numerically integrated between −10 and +14 eV for both the $L_{II}(\Delta A_2)$- and $L_{III}(\Delta A_3)$-edges:

$$f_d = \frac{\Delta A_3 \sigma_3 + 1.11(\Delta A_2 \sigma_2)}{\Delta A_{3r} \sigma_3 + 1.11(\Delta A_{2r} \sigma_2)} \quad (1)$$

The fractional change in the total number of unfilled states in the d band of the sample compared to the number in the platinum foil (f_d) was calculated using eq 1. The areas are normalized by multiplying by the X-ray absorption cross section at the edge jump (σ). Values of 117.1 and 54.2 $cm^2\ g^{-1}$ were used for the absorption cross section at the platinum L_{III}- and L_{II}-edges,[43] respectively. When the number of unfilled d states in the reference material (h_{Tr}) is known (equal to 1.6),[44] the number of unfilled d states in the sample (h_{Ts}) can be calculated from the following equation:

$$h_{Ts} = (1 + f_d) h_{Tr} \quad (2)$$

It is surprising to note that the d band unfilled states for all Pt−Ag/C catalysts are low when compared to the value of the E-tek Pt/C catalyst. Moreover, the values are increasing with an increase in pH of the preparation of the Pt−Ag/C samples (Table 2). This information strongly supports that the electron density around Pt atoms is significantly enhanced due to the partial donation of Ag atoms in the alloyed Pt−Ag/C samples. Ag and Pt are known to possess very near electronegativity scale values, 1.9 and 2.2, respectively, but their charge-transfer scale (*C*-index) shows a significant difference.[45] The *C*-index for Ag is 0.60 and 0.05 for Pt metal, and it may be the origin of charge transfer from Ag to the Pt d-band unfilled states in the Pt−Ag/C alloy nanoparticles. However, the explanation of the increase in d-band unfilled states along with the pH of the

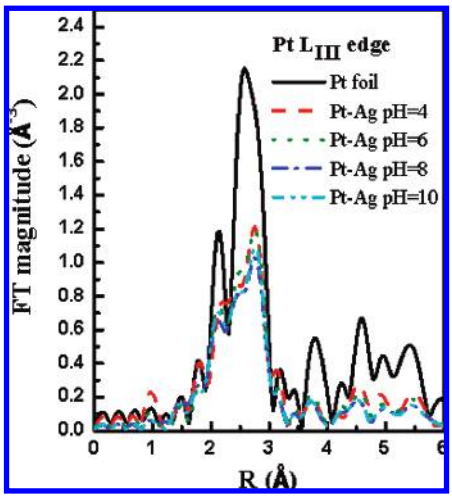

Figure 4. FT-EXAFS spectra for Pt L_{III}-edge of Pt foil and Pt−Ag/C nanoparticles prepared by the EG method.

TABLE 2: Corresponding Fractional Change in the Total Number of Unfilled States in the d Band Compared to the Number in the Platinum Foil (f_d) and the Number of Unfilled d States in the Samples (h_{Ts}) for E-tek Pt/C and Pt−Ag/C Nanoparticles

sample	f_d	h_{Ts}
E-tek Pt/C	0.0060	1.6096
Pt−Ag/C (pH = 4)	−0.00268	1.5957
Pt−Ag/C (pH = 6)	0.00007	1.6001
Pt−Ag/C (pH = 8)	0.00105	1.6017
Pt−Ag/C (pH = 10)	0.00326	1.6052

medium needs more insight into the resultant Pt−Ag/C nanoparticles structure and it will be discussed in detail in a later section.

The EXAFS signal represents the superimposition of contributions of several coordination shells, and thus, the Fourier transform (FT) technique is used to obtain information about the contributions of the individual shells. Peaks in the radial structure of the FT magnitude correspond to the contribution of individual coordination shells around the metallic atom under investigation.[46,47] Figure 4 shows the FT results for the EXAFS oscillations obtained for the Pt L_{III}-edge of all the Pt−Ag/C catalysts and the Pt foil. The peak centered at ca. 2.5 Å in the FT spectra for these materials results from the contributions related to the first Pt−Pt and Pt−Ag coordination shell. Further analyses of the Pt−Ag/C FT-EXAFS results were made from the Pt−Pt and Pt−Ag first coordination shell signals in the Fourier transform. Phase and amplitude data as a function of the radial coordinate were fitted to those calculated for a Pt−Ag/C model using the FEFF program[39] as discussed in the Experimental Section.

Figure 5 represents the Ag K-edge XANES spectra for the Pt−Ag/C nanoparticles which are similar to that of Ag foil. The Ag K-edge FT-EXAFS spectra for various samples are given in Figure 6.

The extracted structural parameters from the EXAFS fitting of Ag K-edge and Pt L_{III}-edges are listed in Table 3. It is quite obvious that with the increase of pH the Pt−Ag coordination number increases are accompanied with a gradual decrease in Pt−Pt coordination. This observation strongly supports that the formation of the Pt−Ag alloy mainly relies on tuning the pH of the preparation medium.

In a recent work from our laboratory we have employed the XAS structural data for the quantitative estimation of extent of alloying or atomic distribution in bimetallic nanoparticles.[23] The

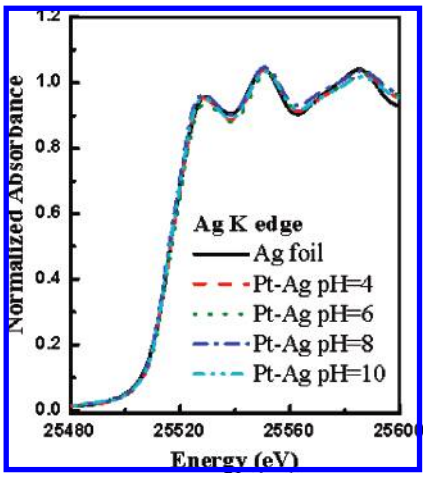

Figure 5. XANES spectra at the Ag K-edge for Ag foil and Pt−Ag/C nanoparticles prepared by the EG method.

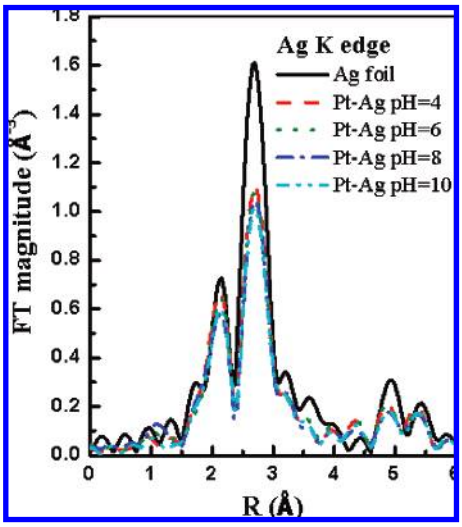

Figure 6. FT-EXAFS spectra for Ag K-edge of Ag foil and Pt−Ag/C nanoparticles prepared by the EG method.

parameters needed to derive the extent of alloying are represented as P_{obsd}, R_{obsd}, P_{random}, and R_{random}. The parameter P_{obsd} can be defined as a ratio of the scattering atoms "Ag" coordination number around absorbing "Pt" atoms (N_{Pt-Ag}) to the total coordination number of absorbing atoms (ΣN_{Pt-i}) ($P_{obsd} = N_{Pt-Ag}/\Sigma N_{Pt-i}$). Similarly, R_{obsd} can be defined as a ratio of the scattering atoms "Pt" coordination number around absorbing "Ag" atoms (N_{Ag-Pt}) to the total coordination number of absorbing atoms (ΣN_{Ag-i}) ($R_{obsd} = N_{Ag-Pt}/\Sigma N_{Ag-i}$). P_{random} and R_{random} can be taken as 0.5 for perfect alloyed bimetallic nanoparticles if the atomic ratio of "Pt" and "Ag" is 1:1. From the ratio of P_{obsd} to P_{random} we can evaluate the extent of alloying of the "Pt" element in the cluster, and similarly from the ratio of R_{obsd} to R_{random} we can estimate the alloying extent of the "Ag" element. The extent of alloying of element "Pt" (J_{Pt}) and element "Ag" (J_{Ag}) for the Pt−Ag bimetallic nanoparticle can be calculated quantitatively by using eqs 3 and 4, respectively:

$$J_{Pt} = \frac{P_{obsd}}{P_{random}} \times 100\% \quad (3)$$

$$J_{Ag} = \frac{R_{obsd}}{R_{Random}} \times 100\% \quad (4)$$

TABLE 3: EXAFS Fitting Parameters at the Pt L_3-Edge and Ag K-Edge for Pt−Ag/C Nanoparticles Prepared by the EG Method

sample	shell	N	R (Å)	$10^3\Delta\sigma_j$	ΔE_0	r-factor
Pt−Ag/C (pH = 4)	Pt−Ag	1.23 (0.09)	2.798 (0.009)	5.3	1.6	0.0038
	Pt−Pt	7.17 (0.12)	2.769 (0.010)	5.8	6.2	
	Ag−Ag	7.01 (0.14)	2.847 (0.009)	8.7	0.3	
	Ag−Pt	1.23 (0.10)	2.798 (0.007)	3.6	−5.2	
Pt−Ag/C (pH = 6)	Pt−Ag	1.43 (0.09)	2.803 (0.009)	5.5	2.7	0.0031
	Pt−Pt	6.46 (0.11)	2.764 (0.008)	6.2	5.6	
	Ag−Ag	6.88 (0.11)	2.841 (0.008)	8.5	1.2	
	Ag−Pt	1.43 (0.12)	2.803 (0.011)	3.4	−3.5	
Pt−Ag/C (pH = 8)	Pt−Ag	1.91 (0.11)	2.808 (0.012)	6.0	2.0	0.0076
	Pt−Pt	6.66 (0.13)	2.770 (0.011)	6.7	6.0	
	Ag−Ag	6.39 (0.14)	2.843 (0.009)	8.6	1.5	
	Ag−Pt	1.91 (0.13)	2.808 (0.012)	5.9	−2.6	
Pt−Ag/C (pH = 10)	Pt−Ag	1.81 (0.12)	2.808 (0.009)	5.4	3.5	0.0047
	Pt−Pt	6.10 (0.13)	2.765 (0.010)	6.6	5.4	
	Ag−Ag	5.75 (0.13)	2.830 (0.010)	8.2	1.3	
	Ag−Pt	1.81 (0.12)	2.808 (0.012)	3.2	−1.8	

TABLE 4: Coordination Number and Alloying Extent Parameters for Pt and Ag Calculated from XAS Experimental Results

sample	ΣN_{Pt-i}	ΣN_{Ag-i}	P_{obsd}	R_{obsd}	J_{Pt} (%)	J_{Ag} (%)	Q value
Pt−Ag/C (pH = 4)	8.40	8.24	0.15	0.15	29.24	29.80	1.02
Pt−Ag/C (pH = 6)	7.89	8.31	0.18	0.17	36.16	34.36	0.95
Pt−Ag/C (pH = 8)	8.57	8.30	0.22	0.23	44.62	46.08	1.03
Pt−Ag/C (pH = 10)	7.91	7.56	0.23	0.24	45.84	47.98	1.05

The lower the J_i value is, the more serious the segregation of i atoms in naoparticles. Table 4 includes the calculated alloying extent values and coordination numbers of individual elements for all the Pt−Ag/C nanoparticles studied in this work. It is quite obvious that the alloying extent values are gradually rising with the medium pH without affecting the Q value of the Pt−Ag/C nanoparticles. Q can represent qualitatively the ratio of surface Ag to Pt atoms in the nanoparticles. The value of Q is greater than 1, suggesting that the surface of the nanoparticles is enriched with Ag atoms. On the contrary, the surface of the nanoparticles would be enriched with Pt atoms if Q was less than 1. The Q values for all the synthesized Pt−Ag/C nanoparticles are nearly equal to 1, indicating the surface compositions of Pt and Ag are similar and independent of pH. This is in fact an extra leverage provided by the EG method if we were able to prepare the Pt−Ag nanoparticles with similar surface compositions but different alloying extents.

From Table 4, it is clear that the alloying extents for Pt and Ag are less than 50% ($J_{Pt,}$ J_{Ag} < 50%) and Σ_{Pt-i} is almost equivalent to Σ_{Ag-i}. Moreover, the coordination number contributed from different shells resembles the sequence of the interaction (H) between atoms (from Table 3) as $H_{Ag-Ag} \sim H_{Pt-Pt} > H_{Pt-Ag}$. Such conditions will favor the formation of the bimetallic nanoparticle with serious segregation[23] from the thermodynamic point of view. However, increasing the reaction kinetics would possibly lead to enhancing the mixing between heteroatoms and increase the alloying extents of atoms in nanoparticles. This is the case for the formation of the Pt−Ag/C nanoparticles prepared by the EG method. It was found that the heteroatomic interactions in the resultant Pt−Ag/C nanoparticles increase with an increase in pH. Certainly this interaction will allow more mixing of Ag and Pt atoms together and tend to increase the alloying extent of Pt and Ag atoms in the resultant clusters.

As mentioned in the previous section, it is appropriate to continue our discussion on the observed trend in the d-band unfilled states of the Pt−Ag/C nanoparticles with respect to the pH of the medium. Figure 7 represents the variations of the d-band unfilled states and the alloying extent values of the Pt−Ag/C catalysts versus their preparation pH. It is quite interesting to note that the increase in alloying extent values of Ag and Pt accompanied with a parallel increase in the d-band unfilled state measured for the respective Pt atoms.

The above observation seems contradictory because of the fact that more alloying of Ag would tend to enhance electron density around Pt which will drastically decrease the d-band vacancy of Pt atoms. However, it is worthwhile to discuss the observed trend in particle size with respect to the preparation pH, and we believe that it will be more appropriate at this juncture. As we mentioned in the previous section, the particle size decreases from 3.1 to 1.2 nm with an increase in pH from 4 to 10. It has been proved that a decrease in particle size of Pt would cause an enhancement in white lines as compared to that of Pt foil because of more vacant 5d orbitals. This in principle can be caused by the smaller particles that have a greater fraction of the Pt atoms at the surface.[48] On the basis of our results and the facts discussed above, the observed the d-band trend may be explained as follows. The increase in the alloying extent of Ag with Pt would tend to supply more electron density (d-band filling) around Pt. On the other hand, a decrease in particle size would lead to empty d-band states. The above said two effects

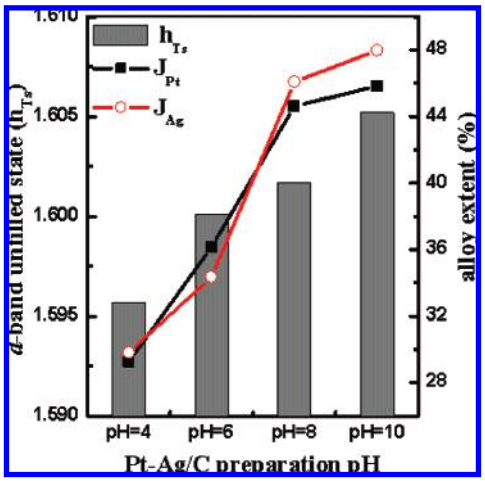

Figure 7. d-band unfilled state and alloy extent values for Pt−Ag/C nanoparticles prepared at various pH values by using the EG method.

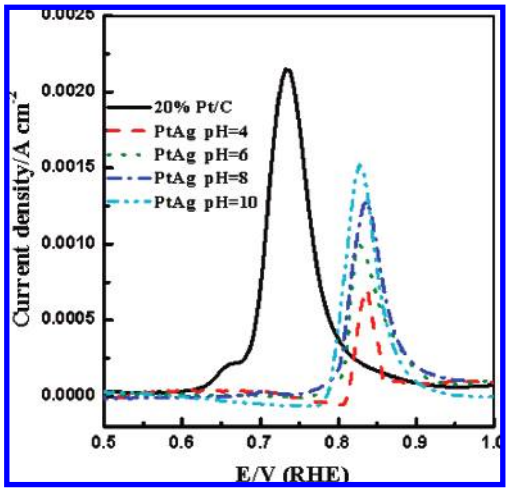

Figure 8. CO stripping voltammograms for Pt/C and Pt−Ag/C nanoparticles in N_2-saturated 0.5 M sulfuric acid electrolyte at 0.005 V s^{-1}.

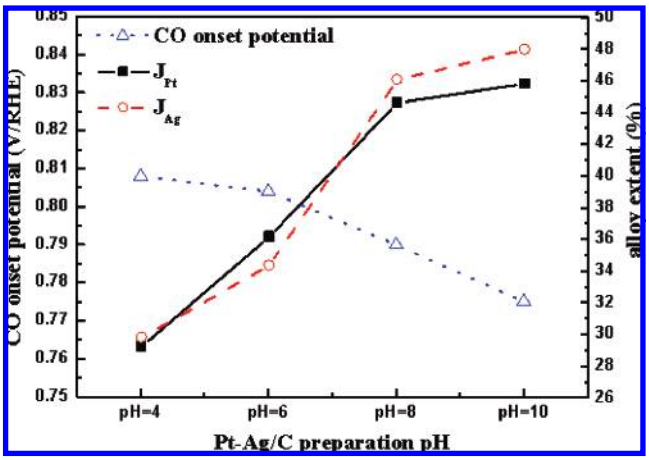

Figure 9. Variation of alloying extents and onset potential for CO stripping of Pt−Ag/C nanoparticles prepared under different pH conditions.

TABLE 5: Electroactive Area and Specific Surface Area of Pt Calculated from CO Stripping Experiments

sample	electroactive area of Pt (m^2)	Pt specific surf area (m^2 g^{-1})
E-tek Pt/C	1.33×10^{-3}	30.62
Pt−Ag (pH = 4)	0.22×10^{-3}	5.00
Pt−Ag (pH = 6)	0.44×10^{-3}	10.22
Pt−Ag (pH = 8)	0.77×10^{-3}	18.14
Pt−Ag (pH = 10)	0.91×10^{-3}	21.07

mutually nullify each other in the Pt−Ag/C nanoparticles, and the observed d-band unfilled states should be a resultant of the two opposite effects.

The CO stripping voltammograms for E-tek Pt/C and Pt−Ag/C nanoparticles are shown in Figure 8. The peak potential for the CO oxidation at the E-tek Pt/C nanoparticle surface was found at 740 mV (RHE), which exactly matches with the previous report of Matsui et al.[49] recorded under similar experimental conditions. The electrochemical active area and specific surface area for Pt calculated from CO stripping charge are listed in Table 5. It is clear that the specific surface area value ca. 30.6 m^2 g^{-1} calculated for the E-tek Pt/C is in good agreement with the value of 36.4 m^2 g^{-1} obtained for JM Pt/C (40% loading)[49] testifies about the reliability of our experimental method. It is interesting to note that the peak potentials for the Pt−Ag/C nanoparticles are shifted to approximately 100 mV positive with respect to that of the Pt/C catalyst. This observation clearly shows that the alloying of Ag with Pt makes the oxidation of CO on Pt surface sluggish. In contrast to Ag, other metals like Ru,[50] Sn,[51] and Mo[52,53] favor CO oxidation by decreasing the oxidation potential significantly on their alloy surfaces. It has been proposed that the above-mentioned metals are capable to reduce the electron density around Pt atoms. A decrease in Pt electron density certainly will encourage CO chemisorption but weakens the back-donation of Pt toward CO.[54] The calculated electroactive area and specific surface area of Pt in the Pt−Ag/C nanoparticles are included in Table 5. The specific surface area for Pt−Ag/C increases with an increase in the preparation pH of the respective nanoparticles. This may be originated from the fact that with increasing pH a decrease in the grain size of Pt−Ag/C (from 3.1 to 1.2 nm) was observed. This in turn enhances the specific surface area as well as the surface population of Pt sites in the given mass of the Pt−Ag/C nanoparticles. This argument can be correlated with the measured electroactive area of Pt (m^2), which is an index of the surface Pt sites increasing with an increase in the pH of the medium.

However, a close inspection of the CO oxidation peaks for the Pt−Ag/C nanoparticles reveals that with increasing alloying extents of Pt and Ag a decrease in onset potential was observed. The trends of alloying extents and onset potential are plotted with respect to the preparation pH of the Pt−Ag/C nanoparticles in Figure 9. This observation is likely to be explained on the basis of the fact that the increase in alloying extent of Ag with Pt leads to an enhancement in electron density around Pt. On the other hand the gradual reduce in grain size of Pt−Ag with increasing pH results in a decrease in the electron density around Pt atoms. At very low grain size, it seems both of the two effects are mutually nullifying toward each other and the calculated net d-band unfilled state is approaching the value of Pt/C. Increasing the alloying extent of Ag with Pt would lead to an increase of the impedance of the CO oxidation reaction on the Pt−Ag nanoparticles with similar size due to the electronic effect. The CO oxidation can be enhanced by reducing the size of Pt−Ag nanoparticles with similar alloying extent. In conclusion, the CO oxidation can be improved by increasing the unfilled states of Pt in the nanoparticles which are associated with electron transfer between heteroatoms and their particle size.

Conclusions

The carbon-supported Pt−Ag alloy nanoparticles have been successfully synthesized by the EG method. The EG method seems to be an efficient method to tune the alloying extent and particle size of the Pt−Ag/C alloy nanoparticles by a fine control over the solution pH. Our observations led us to conclude that the low pH = 4 produces Pt−Ag/C particles of large grain size with poor alloying extent and a wide particle size distribution. It is due to the fact that the homometallic interaction (Ag−Ag and Pt−Pt) is stronger than the heterometallic one (Pt−Ag). At high pH, the reaction kinetics of metal reductions are enhanced and the glycolate availability is also increased in parallel. Therefore, the mixing of Pt and Ag can be improved and the agglomeration of Pt−Ag particles can be prevented simultaneously. Such conditions led the formation of the Pt−Ag particles with smaller grain size, better alloying extent, and a narrow particle size distribution at higher pH. The observed trend of increasing alloying extent with solution pH is quite the reverse for particle size values reported in this work. The

calculated d-band unfilled states for all Pt−Ag/C nanoparticles are low when compared to the value for E-tek Pt/C nanoparticles. However, the values are gradually rising with the pH employed for the preparation of the Pt−Ag/C nanoparticles. It may be due to two effects, namely, electron donations by Ag and size effects operating in the Pt−Ag/C nanoparticles. We proposed that the observed d-band unfilled states should be a resultant of the two opposite effects. In general, the alloying of Ag with Pt leads to the oxidation of CO on the Pt surface becoming sluggish. Among the Pt−Ag/C nanoparticles, an increase in alloying extents of Pt and Ag leading to a decrease in onset potential of CO oxidation was observed, and it may be due to the above-mentioned compensation effects operating in the resultant Pt−Ag clusters.

Acknowledgment. Financial support from the National Science Council under the special program on Nanoscience and Nanotechnology (Grant No. NSC-95-2120-M-011-002) and use of facilities from the National Synchrotron Radiation Research Center (NSRRC) and the National Taiwan University of Science and Technology, Taiwan, ROC, are gratefully acknowledged.

Supporting Information Available: EXAFS spectra. This material is available free of charge via the Internet at http://pubs.acs.org.

References and Notes

(1) De Jongh, L. J., Ed. *Physics and Chemistry of Metal Cluster Compounds*; Kluwer Academic/Plenum Publishers: Dordrecht, The Netherlands, 1994.
(2) Schmid, G., Ed. *Clusters and Colloids From Theory to Applications*; VCH: Weinheim, Germany, 1994.
(3) Fendler, J. H., Ed. *Nanoparticles and Nanostructured Films*; Wiley-VCH: Weinheim, Germany, 1998.
(4) Sugimoto, T., Ed. *Fine Particles*: *Synthesis, Characterizations, and Mechanisms of Growth*; Marcel Dekker: NewYork, 2000.
(5) Liz-Marzan, L. M., Kamat, P. V., Eds. *Nanoscale Materials*; Kluwer Academic/Plenum Publishers: Boston, MA, 2003.
(6) Teranishi, T.; Toshima, N. *Catalysis and Electrocatalysis at Nanoparticle Surfaces*; Wieckowski, A., Sarimone, E. R., Vayenas, C. C., Eds.; Marcel Dekker: New York, 2003; Chapter 11, p 379.
(7) Toshima, N. *Encyclopedia of Nanoscience and Nanotechnology*; Scwarz, J. A., Contescu, C., Putyera, K., Eds.; Marcel Dekker: New York, 2004; p 1869.
(8) Toshima, N.; Yonezawa, T. *New J. Chem.* **1998**, *22*, 1179.
(9) Link, S.; Wang, S. Z. L.; El-Sayed, M. A. *J. Phys. Chem. B* **1999**, *103*, 3529.
(10) Mallin, M. P.; Murphy, C. J. *Nano Lett.* **2002**, *2*, 1235.
(11) Ah, C. S.; Hong, S. D.; Jang, D.-J. *J. Phys. Chem. B* **2001**, *105*, 7871.
(12) Cao, Y.-W.; Jin, R.; Mirkin, C. A. *J. Am. Chem. Soc.* **2001**, *123*, 7961.
(13) Bian, B.; Hirotsu, Y.; Sato, K.; Ohkubo, T.; Makino, A. *J. Electron Microsc.* **1999**, *48*, 753.
(14) Treguer, M.; Cointet, C.; Remita, H.; Khatouri, J.; Mostafavi, M.; Amblard, J.; Belloni, J.; Keyzer, R. *J. Phys. Chem. B* **1998**, *102*, 4310.
(15) Belloni, J.; Mostafavi, M.; Remita, S.; Marignier, J. L.; Delcourt, M. O. *New J. Chem.* **1998**, *22*, 1239.
(16) Smova-Sloufova, I.; Lednicky, F.; Gemperle, A.; Gemperlova, J. *Langmuir* **2000**, *16*, 9928.
(17) Torigoe, K.; Nakajima, Y.; Esumi, K. *J. Phys. Chem.* **1993**, *97*, 8304.
(18) Liz-Marzan, L. M.; Philipse, A. P. *J. Phys. Chem.* **1995**, *99*, 15120.
(19) Doudna, C. M.; Bertino, M. F.; Blum, F. D.; Tokuhiro, A. T.; Lahiri-Dey, D.; Chattopadhyay, S.; Terry, J. *J. Phys. Chem. B* **2003**, *107*, 2966.
(20) Lahiri, D.; Bunker, B.; Mishra, B.; Zhang, Z.; Meisel, D.; Doundna, C. M.; Bertino, M. F.; Blum, F. D., Tokuhiro, A. T.; Chattopadhyay, S.; Shibata, T.; Terry, J. *J. Appl. Phys.* **2005**, *97*, 094304.
(21) Bock, C.; Paquet, C.; Couillard, M.; Botton, G. A.; MacDougall, B. R. *J. Am. Chem. Soc.* **2004**, *126*, 8028.
(22) Sarma, L. S.; Chen, C. H.; Senthil Kumar, S. M.; Wang, G. R.; Yen, S. C.; Liu, D. G.; Sheu, H. S.; Yu, K. L.; Tang, M. T.; Lee, J. F.; Bock, C.; Chen, K. H.; Hwang, B. J. *Langmuir* **2007**, *23*, 5802.
(23) Hwang, B. J.; Sarma, L. S.; Chen, L. M; Chen, C. H.; Shih, S. C.; Wang, G. R.; Liu, D. G.; Lee, J. F.; Tang, M. T. *J. Am. Chem. Soc.* **2005**, *127*, 11140.
(24) Park, J.-I.; Kim, M. G.; Jun, Y.; Lee, J. S.; Lee, W.; Cheon, J. *J. Am. Chem. Soc.* **2004**, *126*, 9072.
(25) Nashner, M. S.; Frenkel, A. I.; Adler, D. L.; Shapley, J. R.; Nuzzo, R. G. *J. Am. Chem. Soc*. **1997**, *119*, 7760.
(26) O'Grady, W. E.; Hagans, P. L.; Pandya, K. I.; Maricle, D. L. *Langmuir* **2001**, *17*, 3047.
(27) Hills, C. W.; Nashner, M. S.; Frenkel, A. I.; Shapley, J. R.; Nuzzo, R. G. *Langmuir* **1999**, *15*, 690.
(28) Nashner, M. S.; Frenkel, A. I.; Somerville, D.; Hills, C. W.; Shapley, J. R.; Nuzzo, R. G. *J. Am. Chem. Soc.* **1998**, *120*, 8093.
(29) Toshima, N.; Harada, M.; Yonezawa, T.; Kushihashi, K.; Asakura, K. *J. Phys. Chem*. **1991**, *95*, 7448.
(30) Bian, C.-R.; Suzuki, S.; Asakura, K.; Ping, L.; Toshima, N. *J. Phys. Chem. B* **2002**, *106*, 8587.
(31) Bazin, D.; Rehr, J. J. *J. Phys. Chem. B* **2003**, *107*, 12398.
(32) Tsai, Y. W.; Tseng, Y. L.; Sarma, L. S.; Liu, D. G.; Lee, J.-F.; Hwang, B. J. *J. Phys. Chem. B* **2004**, *108*, 8148.
(33) Hwang, B.-J.; Tsai, Y. W.; Sarma, L. S.; Liu, D. G.; Lee, J. F. *J. Phys. Chem. B* **2004**, *108*, 20427.
(34) Chen, C.-H.; Hwang, B.-J.; Wang, G.-R.; Sarma, L. S.; Tang, M.-T.; Liu, D.-G.; Lee, J.-F. *J. Phys. Chem. B* **2005**, *109*, 21566.
(35) Chen, C.-H.; Sarma, L. S.; Wang, G. R.; Chen, J. M.; Shih, S. C.; Tang, M. T.; Liu, D. G.; Lee, J. F.; Chen, J. M.; Hwang, B.-J. *J. Phys. Chem. B* **2006**, *110*, 10287.
(36) Hwang, B.-J.; Sarma, L. S.; Wang, G. R.; Chen, C.-H.; Liu, D. G.; Sheu, H. S.; Lee, J. F. *Chem.−Eur. J.* **2007**, *13*, 6255.
(37) (a) See, for example, the guidelines for data collection modes for EXAFS measurements and user controlled parameters: http://ixs.iit.edu/subcommittee_reports/sc/sc00report.pdf. (b) See, for example, the guidelines for error reporting: http://ixs.iit.edu/subcommittee_reports/sc/ err-rep.pdf.
(38) Stern, E. A.; Newville, M.; Ravel, B.; Yacoby, Y.; Haskel, D. *Physica B* **1995**, *208−209*, 117.
(39) Zabinsky, S. I.; Rehr, J. J.; Ankudinov, A. L.; Albers, R. C.; Eller, M. J. *Phys. Rev. B* **1995**, *52*, 2995.
(40) Mukerjee, S.; Srinivasan, S.; Soriaga, M. P. *J. Electrochem. Soc.* **1995**, *142*, 1409.
(41) Reifsnyder, S. N.; Otten, M. M.; Sayers, D. E.; Lamb, H. H. *J. Phys. Chem. B* **1997**, *101*, 4972.
(42) Mansour, A. N.; Cook, J. W.; Sayers. D. E. *J. Phys. Chem.* **1984**, *88*, 2330.
(43) Ramallo-Lopez, J. M.; Santori, G. F.; Giovanetti, L.; Casella, M. L; Ferretti, O. A.; Requejo. F. G. *J. Phys. Chem. B* **2003**, *107*, 11441.
(44) Ankudinov, A. V.; Nesvizhskii, A. I.; Rehr, J. *J. Synchrotron Radiat.* **2001**, *8*, 92.
(45) Jeon, Y.; Chen, J.; Croft, M. *Phys. Rev. B* **1995**, *52*, 2995.
(46) Russell, A. E.; Rose, A. *Chem. Rev.* **2004**, *104*, 4613.
(47) Hwang, B. J.; Tsai, Y. W.; Sarma, L. S.; Chen, C. H.; Lee, J. F.; Strehblow, H. H. *J. Phy. Chem. B*, **2004**, *108*, 15096.
(48) Mukerjee, S.; Urian, R. C. *Electrochim. Acta* **2002**, *47*, 3219.
(49) Matsui, T.; Fujiwara, K.; Okanishi, T.; Kikuchi, R.; Takeguchi, T.; Eguchi, K. *J. Power Sources* **2006**, *155*, 152.
(50) McBreen, J.; Mukerjee, S. *J. Electrochem. Soc.* **1995**, *142*, 3399.
(51) Srinivasan, R.; Davis, B. H. *Platinum Met. Rev.* **1992**, *36*, 151.
(52) Russell, A. E.; Maniguet, S.; Mathew, R. J.; Yao, J.; Roberts, M. A.; Thompsett, D. *J. Power Sources* **2001**, *96*, 226.
(53) Neto, A. O.; Giz, M. J.; Perez, J.; Ticianelli, E. A.; Gonzalez, E. R. *J. Electrochem. Soc.* **2002**, *149*, A272.
(54) Arico, A. S.; Srinivasan, S.; Antonucci, V. *Fuel Cells* **2002**, *1*, 133.